Report

Current Biology

Stabilization of Gaze during Early *Xenopus* Development by Swimming-Related Utricular Signals

Graphical Abstract

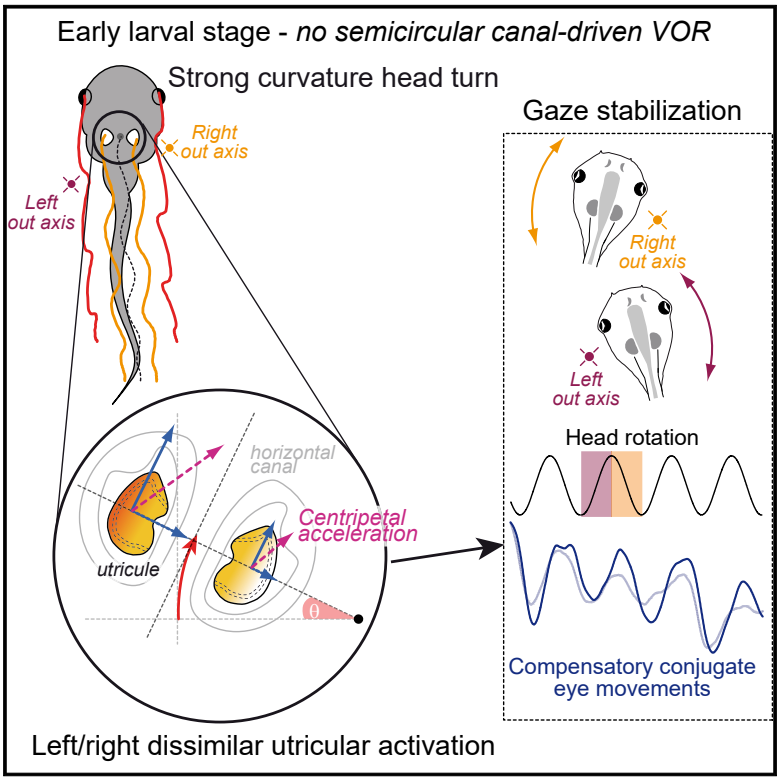

Highlights

- *Xenopus* larvae elicit compensatory, gaze-stabilizing eye movements at all stages
- Swimming in young larvae causes stronger head curvatures and linear acceleration
- Utricular signals during swimming triggers adequate eye movements in young larvae
- Stage-specific locomotor profiles differentially activate vestibular end organs

Authors

François M. Lambert, Julien Bacqué-Cazenave, Anne Le Seach, ..., Selim Eskiizmirliler, Hans Straka, Mathieu Beraneck

Correspondence

francois.lambert@u-bordeaux.fr (F.M.L.), mathieu.beraneck@parisdescartes.fr (M.B.)

In Brief

Lambert, Bacqué-Cazenave, et al. report that swimming in young *Xenopus* larvae generates substantial linear acceleration components, which supplant the incapacity of small semicircular canals to elicit an angular vestibulo-ocular reflex at this stage.

Lambert et al., 2020, Current Biology *30*, 746–753
February 24, 2020
https://doi.org/10.1016/j.cub.2019.12.047

CellPress

CellPress

Current Biology
Report

Stabilization of Gaze during Early *Xenopus* Development by Swimming-Related Utricular Signals

François M. Lambert,[1,4,6,*] Julien Bacqué-Cazenave,[1,4] Anne Le Seach,[2] Jessica Arama,[2] Gilles Courtand,[1] Michele Tagliabue,[2] Selim Eskiizmirliler,[2] Hans Straka,[3,5] and Mathieu Beraneck[2,5,*]
[1]INCIA, CNRS UMR 5287, Université de Bordeaux, F-33076 Bordeaux, France
[2]Integrative Neuroscience and Cognition Center, CNRS UMR 8002, Université de Paris, F-75270 Paris, France
[3]Department Biology II, Ludwig-Maximilians-University Munich, Grosshaderner Str. 2, 82152 Planegg, Germany
[4]These authors contributed equally
[5]These authors contributed equally
[6]Lead Contact
*Correspondence: francois.lambert@u-bordeaux.fr (F.M.L.), mathieu.beraneck@parisdescartes.fr (M.B.)
https://doi.org/10.1016/j.cub.2019.12.047

SUMMARY

Locomotor maturation requires concurrent gaze stabilization improvement for maintaining visual acuity [1, 2]. The capacity to stabilize gaze, in particular in small aquatic vertebrates where coordinated locomotor activity appears very early, is determined by assembly and functional maturation of inner ear structures and associated sensory-motor circuitries [3–7]. Whereas utriculo-ocular reflexes become functional immediately after hatching [8, 9], semicircular canal-dependent vestibulo-ocular reflexes (VORs) appear later [10]. Thus, small semicircular canals are unable to detect swimming-related head oscillations, despite the fact that corresponding acceleration components are well-suited to trigger an angular VOR [11]. This leaves the utricle as the sole vestibular origin for swimming-related compensatory eye movements [12, 13]. We report a remarkable ontogenetic plasticity of swimming-related head kinematics and vestibular end organ recruitment in *Xenopus* tadpoles with beneficial consequences for gaze-stabilization. Swimming of older larvae generates sinusoidal head undulations with small, similar curvature angles on the left and right side that optimally activate horizontal semicircular canals. Young larvae swimming causes left-right head undulations with narrow curvatures and strong, bilaterally dissimilar centripetal acceleration components well suited to activate utricular hair cells and to substitute the absent semicircular canal function at this stage. The capacity of utricular signals to supplant semicircular canal function was confirmed by recordings of eye movements and extraocular motoneurons during off-center rotations in control and semicircular canal-deficient tadpoles. Strong alternating curvature angles and thus linear acceleration profiles during swimming in young larvae therefore represents a technically elegant solution to compensate for the incapacity of small semicircular canals to detect angular acceleration components.

RESULTS

Eye Motion Dynamics during Free-Swimming

The ability of *Xenopus* tadpoles to stabilize gaze during free swimming was evaluated from high-frequency video recordings at two larval stages (stage 47, n = 7; stage 57, n = 5; Figures 1A_1 and 1A_2). Reconstruction of eye-in-space and head-in-space trajectories over several consecutive swim cycles (Figures 1B_1 and 1B_2) revealed that animals at both developmental stages produce conjugate eye movements in phase-opposition to head movements (Figures 1C_1 and 1C_2) with comparable ranges of ocular excursion angles (5°–30°) and degrees of eye-head correlation (Figure 1D). Eye motion magnitudes were maximal (eye-in-head ratio ~1) for small head oscillations (<10°) and minimal (~0.3) for large head oscillations (>40°; Figure 1E), indicating that gaze stabilization is equally effective at both stages and thus independent of larval size or morphometric characteristics. Because tadpoles at the two stages differ in their capacity to encode angular head acceleration [10], potential ontogenetic changes of head motion kinematics were evaluated.

Swim Speed and Head Oscillation Kinematics

Kinematic parameters were obtained from a total of 125 swimming episodes (n = 65 for stage 47; n = 60 for stage 57; 16 animals each). Even though the swim speed of individual animals was rather variable (Figure 1F), older larvae generally swam faster than younger larvae (Figure 1G; $p < 0.001$ Mann-Whitney U test). While the distribution of swim speeds overlapped in the low velocity range, stage 57 tadpoles reached considerably higher velocities compared to stage 47 larvae (Figure 1H) with smaller variance as indicated after normalization to the average speed (Figure 1I).

The capacity to effectively stabilize gaze was estimated by reconstructing head trajectories during swimming (green and blue lines in Figures 2A and 2B) from the highly contrasted outline of the eyeball on each side. While tadpoles at both stages produced left-right head movements during swimming, stage 47 larvae exhibited strong, alternating excursions of the

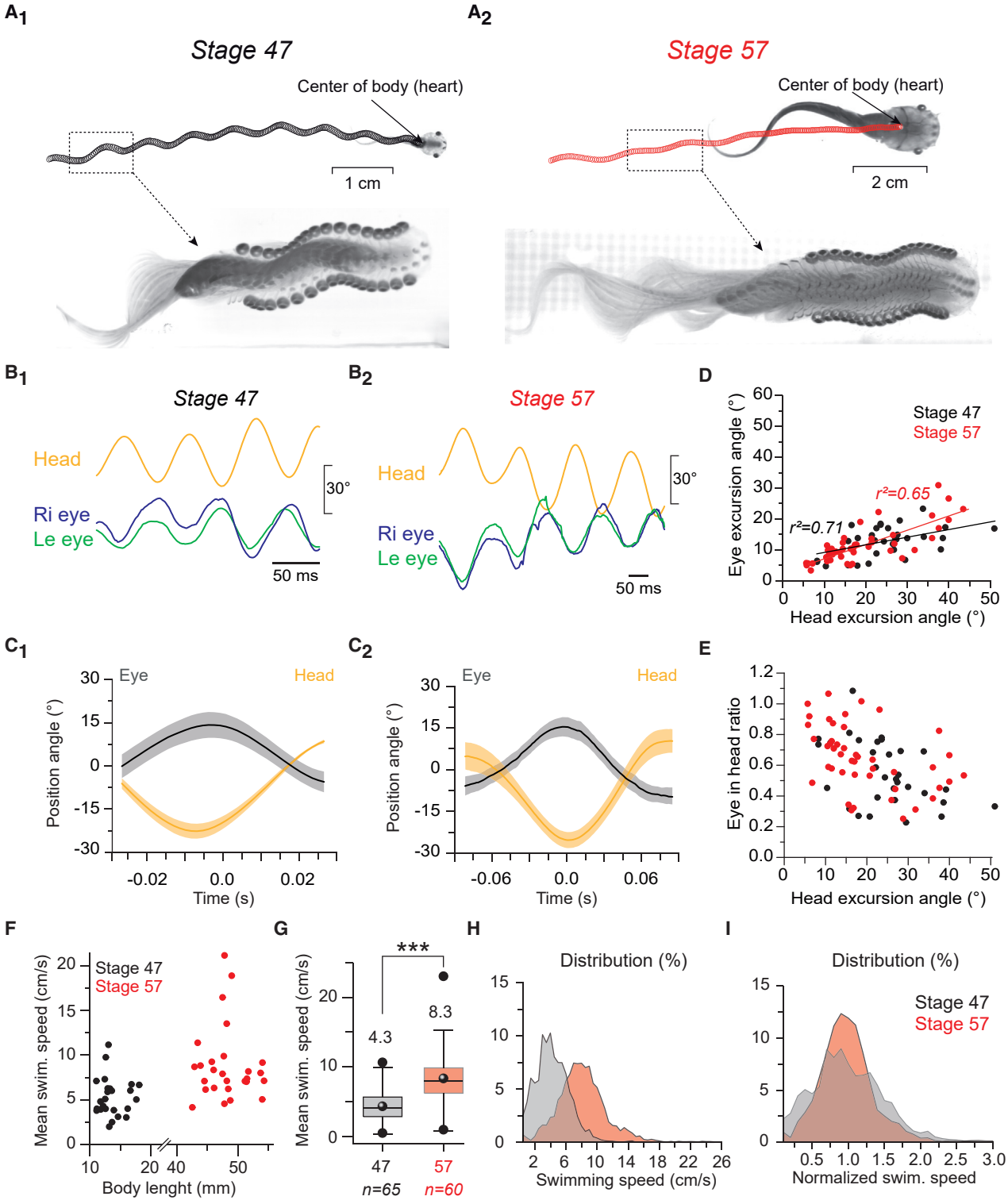

Figure 1. Compensatory Eye Movements During Free Swimming

(A) Frame-by-frame motion trajectory of larval swimming at stage 47 (A_1) and 57 (A_2) obtained from high-speed videos.

(B and C) Representative examples of multiple cycles (B) and average (±SD, shaded area) over a single cycle (C) of swimming-related head and concurrent compensatory movements of the left (Le, green) and right (Ri, blue) eye at stage 47 (B_1 and C_1) and 57 (B_2 and C_2).

(legend continued on next page)

head to both sides (Figures 2A_1–2A_3). During each swim cycle, the eyeball on the inner side of the head turn remained almost stationary in space (green inward marks in Figures 2A_2 and 2A_3). The minimal displacement for ~60 ms (Figure 2C, black trace) corresponded to the low velocity on the side of the inward curve (2.6 ± 1.6 cm/s; Figures 2D and S2E). Simultaneously, the outer side of the head turn (blue outward marks in Figures 2A_2 and 2A_3) advanced considerably farther forward. During the second half cycle, this forward progression profile was inverted (Figure S2E).

At stage 57, the head exhibited a more rectilinear motion pattern (Figures 2B_1–2B_3). During maximal head excursion, the eyeball on the inner side of the head turn moved rather constantly (Figure 2C, red trace) and with a considerably faster velocity (6.4 ± 2.9 cm/s; mean eye velocity $p < 0.001$ Mann-Whitney U test; Figures 2D and S2E) compared to young larvae. Velocities at normalized swimming speed (Figure 2E) confirmed that the inner side of the head turn experienced a longer stationary phase at stage 47 than at stage 57 and thus requires dynamically different compensatory eye movements, which might derive from different sets of vestibular end organs.

Stage-Dependent Swim Motion-Related Acceleration Components

Effective head motion parameters during swimming, as relevant stimulus for vestibular end organs, were calculated from the triangulated trajectories of the inner ears (otic capsule, OC in Figures S1A, S1D, and S1E; Figures 2A and 2B). The heads of stage 47 larvae rotate around alternating eccentric vertical axes located only at a distance of 1–5 mm from the center of the eyeball. This causes the ear on the inner side to follow a narrow curve and on the outer side to proceed along a wider path (Figure 2A_3). Ears of stage 57 tadpoles follow trajectories around rather distant rotation axes (>5 mm) with comparably wide curvature angles (Figure 2B_3). During each head turn, the maximum curvature of the ear on the inner and outer side is thus highly different on the left and right side of the head for each half-cycle at stage 47, but bilaterally more similar at stage 57 (black and red traces in Figures 2F and 2I). This was confirmed after cycle-by-cycle averaging and quantification of the motion trajectory of both ears (Figures 2G, 2H, and 2I; mean maximal curvature, $p < 0.001$ in 2H and $p < 0.0001$ in 2I, Mann-Whitney U test).

The magnitudes of angular acceleration and forward, lateral, and centripetal linear acceleration at peak curvature were calculated separately during each swim cycle at the level of the vestibular end organs (OC; Figures S1E and S3). The more pronounced peak curvature at stage 47 causes considerably larger centripetal linear accelerations (Figures 2J and S3A_4) compared to stage 57, whereas forward, lateral, and angular accelerations were stage-independent (Figures S3B_1–S3B_3). Thus, swimming in young tadpoles causes pronounced left-right-dissimilar centripetal acceleration components, whereas older larvae experience only small, left-right-similar centripetal acceleration components.

Otolith-Ocular Eye Movements as Substitute for Deficient Semicircular Canal-Ocular Reflexes

Eye movements were recorded in head-fixed semi-intact preparations (stage 47, n = 7) in the absence of visual and proprioceptive sensory signals and spinal locomotor efference copies. In stage 47 tadpoles, semicircular canal-evoked eye movements during sinusoidal head-center rotations (1 Hz and ± 120°/s) were absent (Figure 3A_1) as previously reported [10]. In contrast, robust conjugate utricle-derived eye oscillations were recorded during cyclic lateral head translations (Figure 3A_2). To evaluate a utricular contribution to gaze-stabilization during swimming, stage 47 tadpole preparations were rotated around eccentric vertical rotation axes, located 5 mm outside the head, respectively. Such off-center head rotations produced conjugate eye movements with a gain of ~0.2 during both left-out (Figure 3A_3) and right-out rotations (Figure S4B). Despite relatively small gains, eye movements were robust, directionally appropriate, and likely derived from an asymmetric activation of bilateral utricular hair cells corroborating previous results in adult frogs [14]. Recordings of lateral rectus (LR) nerve activity during rotation around different axes (1 Hz; ± 30–240°/s) as more precise functional output confirmed differential horizontal semicircular canals and utricular activation (Figure S4F). The larger discharge modulation during rotation around an eccentric versus centered axis (Figures S4F_2 and S4F_3) likely derives from utricular signals, supporting the conclusions drawn from eye motion recordings.

A predominant if not exclusive utricular origin of swim-related compensatory eye movements was substantiated by two further sets of experiments. First, bilateral injections of 0.5% MS-222 into the otic capsule, known to block vestibular afferent spike discharge [15], reversibly abolished both translational and eccentric rotational motion-evoked eye movements (red traces in Figures 3A_2, 3A_3, and S4C). Second, bilateral semicircular canal-deficient stage 50 larvae were generated by hyaluronidase injections into both otic capsules at stage 44, as previously described in *Xenopus* [16–18]. As confirmation for the absence of bilateral semicircular canals and in compliance with prior studies [17, 18], these animals completely lacked cyclic eye movements during rotation around a centered vertical axis (Figures 3B_1 and 3C_1). However, lateral translation (Figures 3B_2 and 3C_2) as well as rotation around eccentric axes (Figures 3B_3, 3C_3, and S4E) evoked robust, compensatory eye movement. In the absence of all other motion-related sensory signals, these experiments therefore collectively confirm a utricular origin of these eye movements and suggest that the swim style of young tadpoles is able to recruit otolith-ocular pathways for gaze-stabilization.

DISCUSSION

Swimming of stage 47 in contrast to stage 57 larvae is accompanied by strongly curved head trajectories that bilaterally alternate during each swim cycle (Figure 4). The pronounced curvature profile causes considerable centripetal acceleration components and differentially activates utricular signals on both sides that

(D and E) Scatterplots of eye excursion angle (D) and eye-in-head ratio (excursion angles of eye/head, E) as function of the head excursion angle.
(F and G) Mean swim speed as function of body length (F) at stage 47 (n = 25) and stage 57 (n = 27) and distribution of mean (±SD) swim speeds (G); ***$p < 0.001$ (Mann-Whitney U test).
(H and I) Distribution of absolute (H) and normalized average swim speed (I; relative to average swim speed, see G).

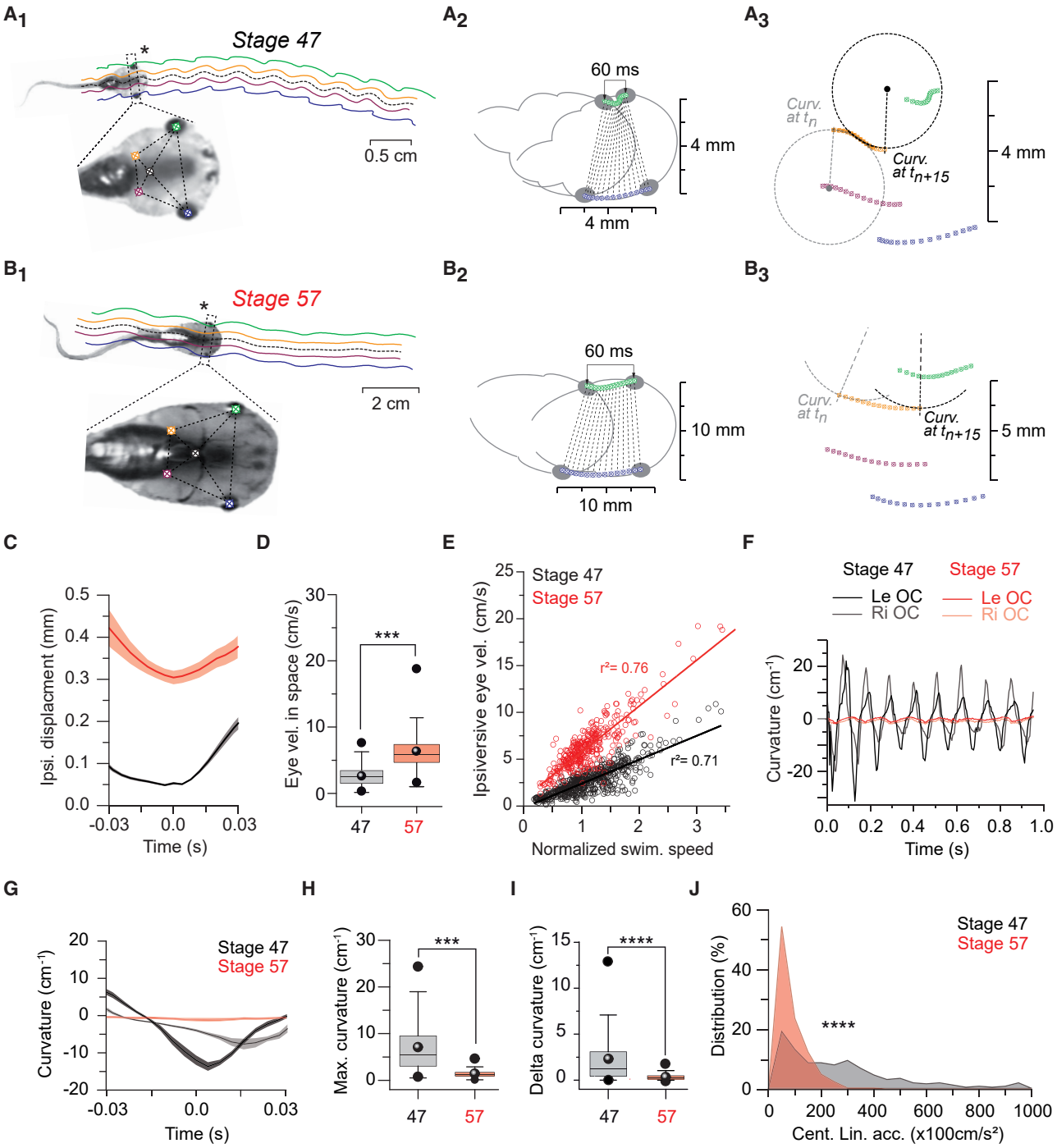

Figure 2. Comparison of Head Motion Trajectories

(A and B) Head trajectory (A_1 and B_1, see Videos S1 and S2); magnified views of the head turn (A_2 and B_2) over a period of 60 ms (dashed rectangular area marked with * in A_1 and B_1) during swimming of stage 47 (A) and 57 (B) tadpoles; note that the displacement of the inner side of the head turn (green) causes the head movements (interconnecting lines between the eyes in A_2 and B_2) to be more accentuated in younger animals; frame-by-frame position of eyeballs and inner ears at the peak of the head turn (A_3 and B_3) indicate the curvature and the direction (dashed lines) on the inner ear from the first to the last image of the 60 ms time window.(C) Trajectory (mean ± SEM) of the inner side of the head turn, averaged over 60 ms at the peak of the rotation (A_2 and B_2) during the swimming episode shown in (A_1 and B_1).

(D) Mean velocity (±SD) of the eye on the inner side of the head turn; note the overall smaller velocity in stage 47 animals; ***$p < 0.001$ (Mann-Whitney U test).

(E) Scatterplot depicting the velocity of the inner side of the head turn as a function of normalized swimming speed (see also Figure S2).

(F) Curvature of the inner ear (otic capsule, OC) on the left (dark red, black) and right inner ear (light red, gray) of the head turn over several swim cycles; note the difference in curvature magnitudes at the two stages and the complete overlap of the trajectories of the inner and outer side (red) at stage 57.

(legend continued on next page)

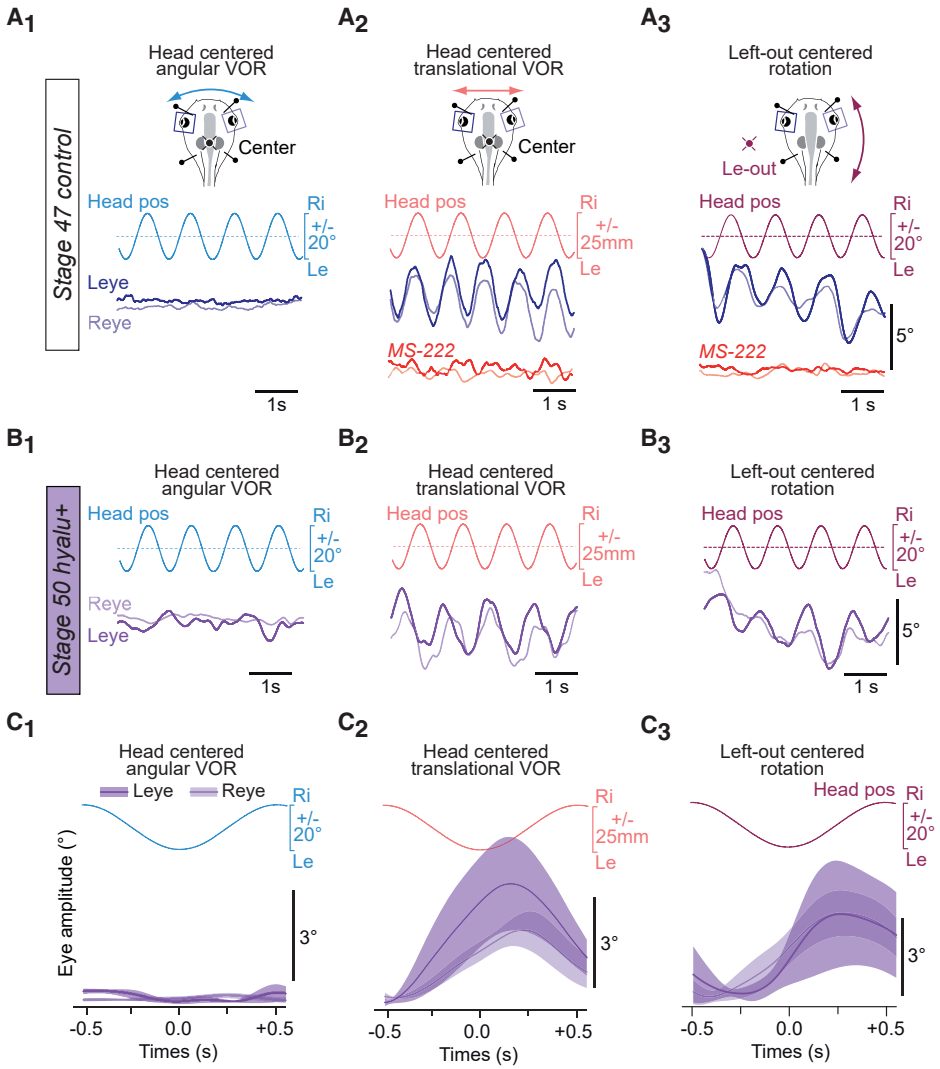

Figure 3. Influence of Rotation Axis Position on Eye Movements in Tadpoles with Intact, Pharmacologically Impaired, or Semicircular Canal-Deficient Inner Ears

(A) Movement of the left (dark traces) and right (light traces) eye at stage 47 during horizontal rotation with the vertical axis in the center (A_1, blue), left-right linear translation (A_2, pink; see Video S3), and during off-center (left-out centered in A_3; Le-out, purple; see Video S4) under control condition (blue traces) and after injection of 0.5% MS-222 into both inner ears (red traces); note that the robust conjugate compensatory eye movements during translation (A_2) and off-center rotation (A_3) were completely abolished by the local anesthetic (see also Figure S4).

(B and C) Four successive motion cycles (B) and average over a single cycle (mean ± SEM, C) of the left (dark traces) and right eye (light traces) during horizontal rotation with the vertical axis in the center (B1 and C1, blue), left-right linear translation (B_2 and C_2, pink), and during off-center (B_3 and C_3; Le-out, purple) in a semicircular canal-deficient stage 50 tadpole (n = 5); note the absence of eye movements during centered vertical-axis rotations and their persistence during off-center rotations and translations (see also Figure S4).

dominate reactive compensatory eye movements, supplanting the negligible angular VORs of young tadpoles.

Developmental Plasticity of Swimming Performance

Tadpoles between stage 47 and 57 experience a 3- to 4-fold increase in body length, whereas the morphometric ratio of several anatomical markers (Figure S1B) and normalized swim speed remain constant. While this suggests similar swimming dynamics and scaling of forward thrust magnitude with increasing tail propulsive capacity, forward motion is achieved by different propulsive dynamics, respectively (Figure 4A). Parameters such as tail thickness and elastic capacity, relevant for tail bending,

(G–I) Curvature (mean ± SEM) of the inner ear on the inner (dark) and outer side (light) of the head turn (G) averaged from the cyclic swim-related head motion shown in (A_1, B_1, and F); mean ± SD of the maximal (H) and Delta curvature (left-right inner ear curvature, I) obtained from all sequences; note that the curvatures of the inner and outer side overlap completely at stage 57 (G); ***p < 0.001, ****p < 0.0001 (Mann-Whitney U test).

(J) Distribution of centripetal linear acceleration at the level of the inner ears during swimming; corresponding distributions of forward, lateral, and angular accelerations are illustrated in Figure S3; ****p < 0.0001 (Kolmogorov-Smirnov test).

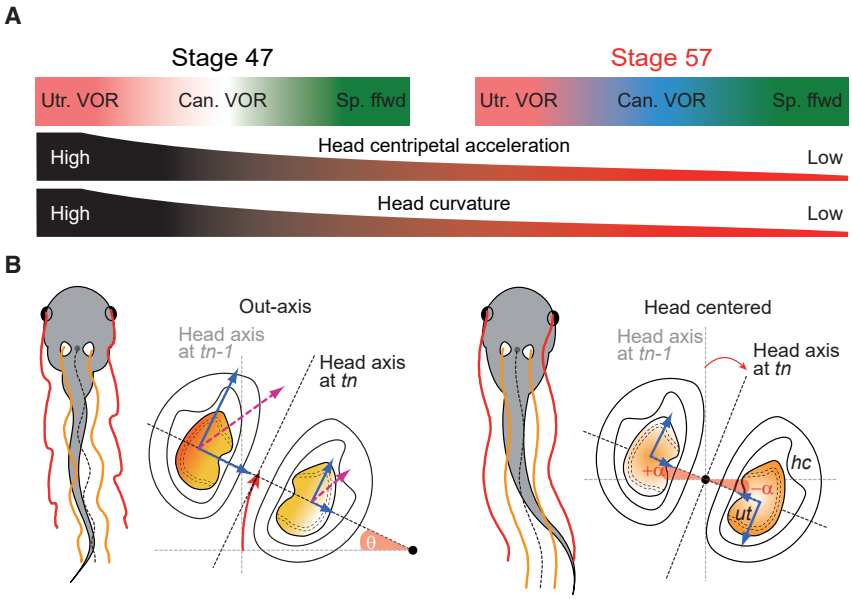

Figure 4. Developmental Plasticity of Locomotor Dynamics and Corresponding Inner Ear Organ Recruitment

(A) Presumed differential activation of the utricle (utr.), semicircular canals (can.), VORs, and spinal feedforward efference copies (Sp. ffwd) during swimming at stage 47 and 57 (upper row) in correspondence with changes of head centripetal acceleration and curvature profiles (lower rows).

(B) Swim pattern and spatial displacement of the bilateral utricle during the different swimming-related head rotations at stage 47 (left) and stage 57 (right) between time *n-1* point (*tn-1* in gray) and time *n* point (*tn* in black); linear, utricular (blue solid arrows); and angular, semicircular canal acceleration components (red solid arrow) are indicated; magenta dashed arrows represent the resulting centripetal linear component during out-axis rotation. α, Θ, angular displacement between *tn-1* and *tn*.

are non-linearly scaled with body growth [11]. Thus, the relatively larger mass of the head and body with respect to the tail [19] and smaller Reynolds numbers of small larvae [20] are obviously more relevant factors for stage-specific swim style dynamics. Independent of head motion kinematics, however, gaze-stabilizing eye movements are generated throughout development.

Role of Predictive Signals for Gaze-Stabilizing Eye Movements

The occurrence of predictable visual perturbations during rhythmic locomotor activity allows gaze-stabilizing eye movements to be evoked by intrinsic copies of the propulsive motor commands [21, 22]. Spinal locomotor efference copies in larval *Xenopus* initiate compensatory eye movements during swimming [11, 23]. While initially demonstrated for mid-larval stages, spino-extraocular motor coupling could also play an important role for gaze-stabilization in young larvae. Compensatory eye movements appear early in development, along with free swimming [24] and the maturation of the underlying spinal network [25]. Despite the peculiar motion trajectory, the stereotypic swim style of young larvae make locomotor efference copies nonetheless suitable to elicit gaze-stabilizing eye movements. This feedforward connectivity is, however, calibrated by vestibular sensory feedback [11, 24], which, during ontogeny, shifts in correspondence with the swim-style-related head motion kinematics from utricular-only to utricular and semicircular canal-based signals.

Role of Vestibular Signals for Gaze-Stabilizing Eye Movements

Gaze-stabilizing eye movements derive from a co-joint activation of semicircular canal and otolith organs [14]. Following vectoral decomposition of angular and linear head and body motion components by the end organs, signals with common spatial field sensitivity converge at the level of central vestibular neurons [26–28]. In compliance with such a fusion, the lateral utricular epithelial sector activates LR and synergistic medial rectus motoneurons in rats [29] and frogs [30] during left-right translational motion to produce conjugate horizontal eye movements comparable to those during yaw-axis head rotation [14]. This extraocular motor pattern is ideally suited to compensate the presumed horizontal image shifts during such head movements and is likely present in all vertebrates [31]. This varies from the general notion that activation of the lateral utricular sector should elicit vertical and oblique eye movements during roll motion [6, 8] and is potentially related to the neuronal computation underlying a disambiguation of tilt and translational motion. The pronounced central convergence of signals from the horizontal semicircular canal and a lateral utricular epithelial sector [26] thus indicates that different VOR components are not transmitted separately but rather share a common pathway. Within this circuitry, the respective acceleration components are transformed into a single spatiotemporally specific extraocular motor output. Thus, compensatory eye movements during head and body motion originate from sensory-motor processing of co-jointly activated angular and linear head acceleration vectors [14].

During ontogeny, the angular and linear VORs become functional with different time courses that depend on the establishment of the neuronal circuitry, computational capacity of individual cellular elements, and physical integrity of the sense organs [1, 3, 5, 7]. In compliance with the simpler structure of otolith organs [32], graviceptive gaze-stabilizing and postural reflexes appear very early during ontogeny [1, 12, 13, 33]. In contrast, the functionality of the angular VOR depends on sufficiently large semicircular canals to allow endolymph flow during head rotation [34–37], which is particularly critical for small vertebrates such as fish or amphibian larvae [9, 10]. This limitation causes the horizontal angular VOR in *Xenopus* tadpoles to become functional only at stage 49 [10], precluding semicircular canal signals as the origin of gaze-stabilizing eye movements prior to this stage.

The absence of a functional angular VOR in young *Xenopus* larvae could be, however, supplanted by a functionally equivalent, otolith-derived VOR, provided that the head motion contains the relevant sensory (i.e., linear acceleration) stimuli. This

assumption is supported by the finding that angular acceleration in the mammalian vestibular system can be encoded by a linear accelerometer [38, 39]. This complies with our finding that adequate compensatory eye movements are activated in semicircular canal-deficient tadpoles (Figures 3B and 3C). In the absence of semicircular canals, the eye-movement-eliciting sensory signals must derive from the utricle(s). Accordingly, activation of utricular signals by bilaterally alternating centripetal, linear acceleration components can evoke spatially specific compensatory eye movements that contribute to offsetting the visual perturbations of swimming-related head motion. The generation of linear acceleration signals during swimming in young *Xenopus* larvae therefore represents a technically elegant solution to overcome the incapacity of small semicircular canals to detect angular acceleration components and to drive an angular VOR.

STAR★METHODS

Detailed methods are provided in the online version of this paper and include the following:

- KEY RESOURCES TABLE
- LEAD CONTACT AND MATERIALS AVAILABILITY
- EXPERIMENTAL MODEL AND SUBJECT DETAILS
- METHOD DETAILS
  - Anatomical landmarks for motion tracking
  - High-speed video tracking of swimming episodes
  - Video recordings and analysis of eye movements in mechanically secured semi-intact head preparations
  - Injection of MS-222 or hyaluronidase in the bilateral otic capsule
  - Electrophysiological recording of extraocular motor nerve spike discharge
- QUANTIFICATION AND STATISTICAL ANALYSIS
  - Analysis of head and otic capsule (inner ear) kinematics
  - High-speed video recordings and analysis of eye movements during episodes of free swimming
  - Statistics
- DATA AND CODE AVAILABILITY

SUPPLEMENTAL INFORMATION

Supplemental Information can be found online at https://doi.org/10.1016/j.cub.2019.12.047.

ACKNOWLEDGMENTS

The authors thank M. Patrice Jegouzo and Philippe Chauvet for their technical help in designing the experiments, and Bruno Della-Gaspera and Lionel Para-Iglesias for their help with tadpole husbandry. The authors thank the Computer-Integrated Systems for Microscopy and Manipulation at the University of North Carolina at Chapel Hill for making the video Spot Tracker version 05.23 available; credit for this software: CISMM at UNC-CH, supported by the NIH NIBIB (NIH 5-P41-RR02170). This work was supported by the ANR grants ANR-08-BLAN-0145-01 and ANR-15-CE32-0007-02 and by the German Science Foundation (STR478/3-1). M.B. and M.T. received support from the Centre National des Etudes Spatiales. F.M.L. received support from the INCIA CNRS UMR5287.

AUTHOR CONTRIBUTIONS

Conceptualization: F.M.L., H.S., and M.B.; Methodology: F.M.L., J.B.C., A.L.S., J.A., G.C., M.T., S.E., H.S., and M.B.; Software: A.L.S., G.C., M.T., and S.E.; Formal Analysis: F.M.L., J.B.C., A.L.S., J.A., G.C., S.E., and M.B.; Investigation: F.M.L., J.B.C., A.L.S., J.A., and M.B.; Writing – Original Manuscript: F.M.L., S.E., H.S., and M.B.; Writing – Review & Editing: F.M.L., J.B.C., M.T., H.S., and M.B.; Visualization: F.M.L., J.B.C., J.A., S.E., H.S., and M.B.; Supervision: F.M.L., H.S., and M.B.; Project Administration: F.M.L. and M.B.; Funding Acquisition: F.M.L., H.S., and M.B.

DECLARATION OF INTERESTS

The authors declare no competing interests.

Received: August 12, 2019
Revised: November 26, 2019
Accepted: December 13, 2019
Published: January 16, 2020

REFERENCES

1. Straka, H. (2010). Ontogenetic rules and constraints of vestibulo-ocular reflex development. Curr. Opin. Neurobiol. *20*, 689–695.
2. Bagnall, M.W., and Schoppik, D. (2018). Development of vestibular behaviors in zebrafish. Curr. Opin. Neurobiol. *53*, 83–89.
3. Glover, J.C. (2003). The development of vestibulo-ocular circuitry in the chicken embryo. J. Physiol. Paris *97*, 17–25.
4. Wolf, S., Dubreuil, A.M., Bertoni, T., Böhm, U.L., Bormuth, V., Candelier, R., Karpenko, S., Hildebrand, D.G.C., Bianco, I.H., Monasson, R., and Debrégeas, G. (2017). Sensorimotor computation underlying phototaxis in zebrafish. Nat. Commun. *8*, 651.
5. Migault, G., van der Plas, T.L., Trentesaux, H., Panier, T., Candelier, R., Proville, R., Englitz, B., Debrégeas, G., and Bormuth, V. (2018). Whole-Brain Calcium Imaging during Physiological Vestibular Stimulation in Larval Zebrafish. Curr. Biol. *28*, 3723–3735.e6.
6. Bianco, I.H., Ma, L.H., Schoppik, D., Robson, D.N., Orger, M.B., Beck, J.C., Li, J.M., Schier, A.F., Engert, F., and Baker, R. (2012). The tangential nucleus controls a gravito-inertial vestibulo-ocular reflex. Curr. Biol. *22*, 1285–1295.
7. Favre-Bulle, I.A., Vanwalleghem, G., Taylor, M.A., Rubinsztein-Dunlop, H., and Scott, E.K. (2018). Cellular-Resolution Imaging of Vestibular Processing across the Larval Zebrafish Brain. Curr. Biol. *28*, 3711–3722.e3.
8. Horn, E., Lang, H.G., and Rayer, B. (1986). The development of the static vestibulo-ocular reflex in the southern clawed toad, Xenopus laevis. I. Intact animals. J. Comp. Physiol. A Neuroethol. Sens. Neural Behav. Physiol. *159*, 869–878.
9. Beck, J.C., Gilland, E., Tank, D.W., and Baker, R. (2004). Quantifying the ontogeny of optokinetic and vestibuloocular behaviors in zebrafish, medaka, and goldfish. J. Neurophysiol. *92*, 3546–3561.
10. Lambert, F.M., Beck, J.C., Baker, R., and Straka, H. (2008). Semicircular canal size determines the developmental onset of angular vestibuloocular reflexes in larval *Xenopus*. J. Neurosci. *28*, 8086–8095.
11. Bacqué-Cazenave, J., Courtand, G., Beraneck, M., Lambert, F.M., and Combes, D. (2018). Temporal relationship of ocular and tail segmental movements underlying locomotor-induced gaze stabilization during undulatory swimming in larval Xenopus. Front. Neural Circuits *29*, https://doi.org/10.3389/fncir.2018.00095.
12. Mo, W., Chen, F., Nechiporuk, A., and Nicolson, T. (2010). Quantification of vestibular-induced eye movements in zebrafish larvae. BMC Neurosci. *11*, 110.
13. Favre-Bulle, I.A., Stilgoe, A.B., Rubinsztein-Dunlop, H., and Scott, E.K. (2017). Optical trapping of otoliths drives vestibular behaviours in larval zebrafish. Nat. Commun. *8*, 630.

14. Straka, H., and Dieringer, N. (2004). Basic organization principles of the VOR: lessons from frogs. Prog. Neurobiol. *73*, 259–309.
15. Ramlochansingh, C., Branoner, F., Chagnaud, B.P., and Straka, H. (2014). Efficacy of tricaine methanesulfonate (MS-222) as an anesthetic agent for blocking sensory-motor responses in Xenopus laevis tadpoles. PLoS ONE *9*, e101606.
16. Haddon, C.M., and Lewis, J.H. (1991). Hyaluronan as a propellant for epithelial movement: the development of semicircular canals in the inner ear of Xenopus. Development *112*, 541–550.
17. Branoner, F., and Straka, H. (2015). Semicircular canal-dependent developmental tuning of translational vestibulo-ocular reflexes in Xenopus laevis. Dev. Neurobiol. *75*, 1051–1067.
18. Branoner, F., and Straka, H. (2018). Semicircular Canal Influences on the Developmental Tuning of the Translational Vestibulo-Ocular Reflex. Front. Neurol. *9*, 404.
19. Hänzi, S., and Straka, H. (2017). Developmental changes in head movement kinematics during swimming in Xenopus laevis tadpoles. J. Exp. Biol. *220*, 227–236.
20. Liu, H., Wassersug, R., and Kawachi, K. (1996). A computational fluid dynamics study of tadpole swimming. J. Exp. Biol. *199*, 1245–1260.
21. Chagnaud, B.P., Simmers, J., and Straka, H. (2012). Predictability of visual perturbation during locomotion: implications for corrective efference copy signaling. Biol. Cybern. *106*, 669–679.
22. Straka, H., Simmers, J., and Chagnaud, B.P. (2018). A New Perspective on Predictive Motor Signaling. Curr. Biol. *28*, R232–R243.
23. Lambert, F.M., Combes, D., Simmers, J., and Straka, H. (2012). Gaze stabilization by efference copy signaling without sensory feedback during vertebrate locomotion. Curr. Biol. *22*, 1649–1658.
24. Bacque-Cazenave, J., Lambert, F.M., Cayrel, M., Courtand, G., Beraneck, M., and Combes, D. (2017). Quantifying the spinal locomotor network-driven oculomotor behavior and its developmental adaptation in frog. In Proceedings of the Annual Meeting of Society for Neuroscience, Washington, DC.
25. Sillar, K.T., Wedderburn, J.F., and Simmers, A.J. (1991). The development of swimming rhythmicity in post-embryonic Xenopus laevis. Proc. Biol. Sci. *246*, 147–153.
26. Straka, H., Holler, S., and Goto, F. (2002). Patterns of canal and otolith afferent input convergence in frog second-order vestibular neurons. J. Neurophysiol. *88*, 2287–2301.
27. Bush, G.A., Perachio, A.A., and Angelaki, D.E. (1993). Encoding of head acceleration in vestibular neurons. I. Spatiotemporal response properties to linear acceleration. J. Neurophysiol. *69*, 2039–2055.
28. Uchino, Y., Sasaki, M., Sato, H., Bai, R., and Kawamoto, E. (2005). Otolith and canal integration on single vestibular neurons in cats. Exp. Brain Res. *164*, 271–285.
29. Hess, B.J., and Dieringer, N. (1991). Spatial organization of linear vestibuloocular reflexes of the rat: responses during horizontal and vertical linear acceleration. J. Neurophysiol. *66*, 1805–1818.
30. Rohregger, M., and Dieringer, N. (2002). Principles of linear and angular vestibuloocular reflex organization in the frog. J. Neurophysiol. *87*, 385–398.
31. Straka, H., and Baker, R. (2013). Vestibular blueprint in early vertebrates. Front. Neural Circuits *7*, 182.
32. Fritzsch, B., and Straka, H. (2014). Evolution of vertebrate mechanosensory hair cells and inner ears: toward identifying stimuli that select mutation driven altered morphologies. J. Comp. Physiol. A Neuroethol. Sens. Neural Behav. Physiol. *200*, 5–18.
33. Ehrlich, D.E., and Schoppik, D. (2019). A primal role for the vestibular sense in the development of coordinated locomotion. eLife *8*, e45839.
34. Muller, M. (1999). Size limitations in semicircular duct systems. J. Theor. Biol. *198*, 405–437.
35. Rabbitt, R.D., Damiano, E.R., and Grant, J.W. (2004). Biomechanics of the vestibular semicircular canals and otolith organs. In The vestibular system, S.M. Highstein, R.R. Fay, and A.N. Popper, eds. (New York: Springer), pp. 153–201.
36. Hullar, T.E. (2006). Semicircular canal geometry, afferent sensitivity, and animal behavior. Anat. Rec. A Discov. Mol. Cell. Evol. Biol. *288*, 466–472.
37. Yang, A., and Hullar, T.E. (2007). Relationship of semicircular canal size to vestibular-nerve afferent sensitivity in mammals. J. Neurophysiol. *98*, 3197–3205.
38. Angelaki, D.E. (1992). Vestibular neurons encoding two-dimensional linear acceleration assist in the estimation of rotational velocity during off-vertical axis rotation. Ann. N Y Acad. Sci. *656*, 910–913.
39. Angelaki, D.E. (1992). Two-dimensional coding of linear acceleration and the angular velocity sensitivity of the otolith system. Biol. Cybern. *67*, 511–521.
40. Nieuwkoop, P.D., and Faber, J. (1994). Normal table of *Xenopus laevis* (Daudin): a systematical and chronological survey of the development from the fertilized egg till the end of metamorphosis (New York: Garland).
41. Eatock, R.A., Corey, D.P., and Hudspeth, A.J. (1987). Adaptation of mechanoelectrical transduction in hair cells of the bullfrog's sacculus. J. Neurosci. *7*, 2821–2836.
42. von Uckermann, G., Lambert, F.M., Combes, D., Straka, H., and Simmers, J. (2016). Adaptive plasticity of spino-extraocular motor coupling during locomotion in metamorphosing Xenopus laevis. J. Exp. Biol. *219*, 1110–1121.

STAR★METHODS

KEY RESOURCES TABLE

REAGENT or RESOURCE	SOURCE	IDENTIFIER
Chemicals, Peptides, and Recombinant Proteins		
MS-222	Sigma-Aldrich, France	886-86-2
Hyaluronidase	Sigma-Aldrich, France	H1136-1AMP
Deposited Data		
Raw data and videos	This paper, Mendeley data	Mendeley dataset CURRENT-BIOLOGY-D-19-01330 https://doi.org/10.17632/gn6pnsnkvm.1
Experimental Models: Organisms/Strains		
Xenopus laevis larva	Centre de Ressources Biologiques Xénopes, UMS 3387, CNRS, Rennes France	N/A
Software and Algorithms		
Software	This paper, mendeley data	Mendeley dataset CURRENT-BIOLOGY-D-19-01330 https://doi.org/10.17632/gn6pnsnkvm.1
MATLAB2014b, 2018a MathWorks https://www.mathworks.com/products/MATLAB.html	MATLAB2014b, 2018a MathWorks https://www.mathworks.com/products/MATLAB.html	MATLAB2014b, 2018a MathWorks https://www.mathworks.com/products/MATLAB.html
CED 1401, Signal, Spike 2; Cambridge Electronic Design	Cambridge Electronic Design	http://ced.co.uk/products/spkovin
Dataview	St-Andrew University	https://www.st-andrews.ac.uk/∼wjh/dataview/
Custom-build software with Python 3.5	IMAGYS core facility INCIA CNRS UMR 5287	http://www.incia.u-bordeaux1.fr/spip.php?article629
Other		
Digital camera MemView	MemView, Southern Vision Systems Inc., USA	N/A
60mm lens 1:2.8D, and 50mm lens 1:1.8D lens AF NIKKOR,	Nikon, Japan	https://www.nikon.com/
Digital camera Basler ac1920	Basler AG An der Strusbek 60 – 6222926 AhrensburgGermany	https://www.baslerweb.com/en/
Optem MVZL macro video zoom lens, QIOPTIQ	QIOPTIQ	http://www.qioptiq.com/

LEAD CONTACT AND MATERIALS AVAILABILITY

Further information and requests for resources should be directed to and will be fulfilled by the Lead Contact, François Lambert (François.Lambert@u-bordeaux.fr). This study did not generate unique reagents.

EXPERIMENTAL MODEL AND SUBJECT DETAILS

Animals were obtained from an authorized supplier (Centre de Ressources Biologiques *Xénopes*, UMS 3387, CNRS, Rennes France) and kept in the laboratory in filtered water at 18°C until use for experimentation. Experiments were conducted on *Xenopus laevis* tadpoles of either sex (n = 72) at developmental stages 47, 50, 52 and 57 [40] and complied with the ''Principles of Animal Care,'' publication No. 86-23, revised 1985 by the National Institute of Health. Experimental protocols were approved by the local ethical committee for animal research at the Université Paris Descartes (#3301100012-A) and the University of Bordeaux (#2016011518042273 APAFIS #3612).

METHOD DETAILS

Anatomical landmarks for motion tracking

To faithfully track head and concurrent eye movements during free swimming in *Xenopus* tadpoles (see Figure 1), animals were subjected to a topographic mapping of selected anatomical markers prior to the conduction of behavioral experiments. The position of both eyes and otic capsules (OC, inner ears) in the head as well as the heart as a reference for the center of the body was determined in each animal (Figure S1A). These parameters allowed triangulation of the anatomical distances between the eyes and the center of the OCs and their positions relative to each other and to the heart. To obtain these reference markers, tadpoles were anesthetized in 0.03% 3-aminobenzoic acid ethyl ester (MS-222; Pharmaq Ltd., Fordingbridge, Hampshire, UK) in water. Animals were secured to the bottom of a small Petri dish and images were taken from the dorsal and ventral side (MemView Camera, Southern Vision Systems Inc., USA; 60 mm lens 1:2.8D, AF NIKKOR, Nikon, Japan; Resolution: 1024 × 1024 pixels; Figure S1A). Images were processed offline using analysis software (ImageJ) to determine the distances between the different anatomical markers in stage 47 (n = 24) and stage 57 tadpoles (n = 20; Table 1). To compensate for potential inter-individual variations in body size, data were normalized to the inter-ocular distance. This procedure showed that the relative distance between the otic capsules and the heart or the eyes and the otic capsules is very similar at both developmental stages (Table 1; Figure S1B). Based on the better view of the eyes from the ventral side, swimming episodes were video-tracked with the camera positioned underneath the tank (Figure S1C). The reconstruction of head and eye movements and the position of both OCs by automated offline analyses (see below) were performed on the basis of the pre-determined distances of the respective anatomical structures prior to the video tracking (Figure S1A).

Anatomical Features for Larval Stages 47 and 57

Anatomical feature	Stage 47 (in mm)	Stage 47 (normalized)	Stage 57 (in mm)	Stage 57 (normalized)
Eye-Eye	4.1 ± 0.4	1	9.4 ± 0.4	1
Otic capsule-Heart	1.3 ± 0.2	0.4	3.4 ± 0.4	0.38
Eye-Otic capsule	2.1 ± 0.3	0.53	4.6 ± 0.6	0.52
Eye-Heart	2.8 ± 0.3	0.68	5.3 ± 0.02	0.57

Anatomical feature table: Anatomical features were studied in stage 47 (n = 24) and stage 57 tadpoles (n = 20). Distances between the different anatomical markers shown in Figure S1B are reported in mm for stage 47 (first column) and stage 57 (third column), and normalized to the individual inter-ocular distance (second and fourth column for stage 47 and 57, respectively). Note that the relative distance between the otic capsules and the heart or the eyes and the otic capsules is constant despite the body growth.

High-speed video tracking of swimming episodes

Tracking of swimming episodes and eye movements was performed in two complementary recording sessions: a first set of experiments aimed at high spatial and temporal resolution of swimming sequences in order to track eye movements during free swimming. A second set of experiments aimed at tracking the motion kinematics during longer swimming episodes. Accordingly, the motion kinematics of the head, eye and heart in space during free swimming was studied in animals (stage 47, n = 24; stage 57, n = 20) that were placed in a Plexiglas tank (5 × 25 cm) with a water depth of 5 cm. Video sequences were recorded with a digital camera (MemView, Southern Vision Systems Inc., USA), positioned underneath the tank (Figure S1C). Eye movements were tracked by placing the camera as close as possible to the ventral surface of the tank to restrain the field of view and to increase the spatial resolution. A 60 mm lens (1:2.8D, AF NIKKOR, Nikon, Japan) was used to monitor magnified views of the animals. A wide-angle lens (50 mm 1:1.8D lens AF NIKKOR, Nikon, Japan) was used to capture longer swimming episodes and to extract the kinematics of swimming-related head movements. Light sources (Barefly 200, KINOFLO Lighting system; Figure S1A) were placed underneath the tank and oriented such that variations in light reflections were minimal. A second light source (LED LitePad HO (15 × 30 cm, Rosco, USA) was placed above the pool to provide a homogeneous white illuminated background (Figure S1C). To account for size differences between animals at stage 47 and 57 [19], the distance between camera and tank was adjusted to maintain a similar relative image size of the animal (determined by the inter-ocular distance). Eye and head movements were recorded during separate swimming episodes at an image acquisition rate of 750 and 250 frames per seconds (fps), respectively. Swimming episodes lasted for up to 20 tail oscillations (Figure S1D). Only uninterrupted episodes of free swimming that consisted of at least 5 consecutive cycles of tail undulations were further analyzed. The analysis was restricted to swimming episodes that occurred in the horizontal plane, i.e., without concurrent roll motion. Head/body roll movements during swimming were detected in the video recordings by calculating the distance between the two eyes. Episodes in which the individual, pre-determined inter-ocular distance cyclically varied by more than 1% (corresponding to ~8° vertical oscillations of the head) due to roll movements were excluded from the analysis. See Videos S1 and S2 (also deposited at Mendeley: https://doi.org/10.17632/gn6pnsnkvm.1)

Video recordings and analysis of eye movements in mechanically secured semi-intact head preparations

Experiments on semi-intact head preparations served to isolate otolith-related eye movements during specific motion stimulation paradigms. All procedures were performed according to the protocol by Bacqué-Cazenave et al. [11]. In brief, *Xenopus* larvae at stage 47 (n = 5) were anesthetized in a 0.05% MS-222 solution and placed in oxygenated (95% O_2, 5% CO_2) Ringer solution. The temperature of the bath solution was maintained at 18°C. Viscera and forebrain were removed, the brainstem was exposed to give access to the Ringer solution and the tail was removed at the level of the upper spinal cord. To abolish visual sensory inputs, both optic nerves were transected and the semi-intact preparation was firmly secured onto the Sylgard floor of a chamber with insect pins.

The chamber with the preparation was mounted onto a computer-controlled, motorized motion stimulation device that allowed placement of the recording chamber either in the center or at off-center positions with respect to the vertical axis of the stimulator (turntable and sled, Technoshop COH@BIT, IUT de Bordeaux, University of Bordeaux). Motion stimuli consisted of sinusoidal translations at 1 Hz ± 25 mm along the transverse axis, or of sinusoidal rotations at a frequency of 1 Hz and peak stimulus velocities that ranged from ± 30°/s to ± 240°/s with the rotation axis either centered between the two OCs or located laterally outside the head (5 mm).

Left- and rightward directed eye movements were video-recorded from top at 200 fps with a high-speed digital camera (Basler, ac1920) equipped with a micro-inspection lens system (Optem MVZL macro video zoom lens, QIOPTIQ). Automatic tracking of eye motion segments was performed using a custom-built software written in Python 3.5 environment (IMAGYS core facility, INCIA UMR CNRS 5287). For eye movement measurements, a ROI was drawn around each eye and a binary threshold was applied before tracking the angle between the minor axis of the eye ellipse and the head axis. See Videos S3 and S4 (also deposited at Mendeley: https://doi.org/10.17632/gn6pnsnkvm.1)

Raw data from video recordings were processed offline and analyzed with Dataview (by W.J. Heitler, University of St Andrews, Scotland). For video image processing, traces of angular movements of the eyes were first filtered with a 25 Hz low-pass filter. Thereafter, maximal angular excursions of the eyes (peak sinewave) were detected for each individual motion cycle and used to calculate the amplitude of eye movements.

Injection of MS-222 or hyaluronidase in the bilateral otic capsule

After video recordings of eye movements in stage 47 semi-intact head preparation under control conditions (n = 6; see Figure 3A), a calibrated 10 nL volume of a 0.5% MS-222 solution dissolved in artificial endolymph Ringer solution [10, 41] was injected into both otic capsules, respectively. The injection was performed by inserting a beveled microelectrode (30°, 10-15 μm tip diameter; GB150F-8P, Science Products GmbH, Germany) inserted into the center of the transparent otic capsule with a micromanipulator under visual control. The calibrated volume of 10 nL was pressure-injected (0.5 bar, 5 s) with a PICOSPRITZER III pressure injector (Intracel, UK). To prevent the developmental formation of semicircular canals on both sides, a previous established method was employed [16–18]. Accordingly, a calibrated volume (10 nl) of a hyaluronidase enzyme solution (0.5 mg/mL, Sigma-Aldrich, France), dissolved in artificial endolymph Ringer solution was injected into bilateral otic capsules of tadpoles at stage 44 (n = 5). Subsequently, animals were allowed to develop into older stages.

Electrophysiological recording of extraocular motor nerve spike discharge

Recording of extraocular motor nerve activity was performed *in vitro* in semi-intact preparations of stage 50 (n = 4) *Xenopus* tadpoles as described previously [10, 23]. In brief, animals were deeply anesthetized in a cold (4-6°C) solution of 0.05% MS-222 in frog Ringer (75 mM NaCl, 25 mM $NaHCO_3$, 2 mM $CaCl_2$, 2 mM KCl, 0.5 mM $MgCl_2$, and 11 mM glucose, pH 7.4) and decapitated at the level of the upper spinal cord. The skin covering the dorsal region of the head was removed, the soft skull tissue opened and the forebrain disconnected. This surgical procedure anatomically preserved the remaining central nervous system, bilateral inner ear end organs in the OCs including the VIIIth nerves as well as the extraocular motor nerves and eye muscle innervations [10]. After selective disconnection of the abducens nerve from the lateral rectus (LR) target muscle, preparations were transferred to a Sylgard-lined Petri dish (volume 5 ml), and continuously superfused with oxygenated Ringer solution at a rate of 1.5 - 2.1 mL/min and a temperature of 17°C ± 0.1°C.

Multi-unit spike discharge of the LR nerve was recorded with glass suction microelectrodes, produced with a horizontal puller (P-87 Brown/Flaming, Sutter Instruments Company, Novato, CA, USA). Electrode tips were broken and individually adjusted to fit the LR nerve diameter. Natural activation of vestibular end organs was performed with a computer-controlled, motorized two-axis turntable (ACT-1002, Acutronic USA Inc., Switzerland) as described previously [10, 23]. The recording chamber with the preparation was mounted onto a custom-built plate that allowed placement of the recording chamber either in the center or at off-center positions with respect to the vertical axis of the turntable. Accordingly, the rotational axis was either centered between the two OCs or located laterally outside the head. This configuration allowed recordings of LR nerve spike discharge during centered or off-center vertical-axis head rotations. Motion stimuli consisted of sinusoidal oscillations at a frequency of 1 Hz and a peak stimulus velocity that ranged from ± 30°/s to ± 240°/s. Spontaneous and evoked multi-unit LR nerve spike discharges were recorded (Ext 10-2F; npi Electronics, Tamm, Germany), digitized (10 kHz), stored on a computer and analyzed offline (CED 1401, Signal, Spike 2; Cambridge Electronic Design). The magnitude of the discharge modulation was determined by calculating the difference between minimum and maximum firing rates of the averaged discharge over a single turntable motion cycle [10].

QUANTIFICATION AND STATISTICAL ANALYSIS

Analysis of head and otic capsule (inner ear) kinematics

Custom image processing and analysis software was developed in MATLAB to track head and eye movements in video recordings and to determine 2-D spatial positions (X-Y coordinates) of the left and right eye based on a frame-by-frame analysis with the Video Spot Tracker 5.3 (credit: CISMM at UNC-CH; see acknowledgments). Predetermined anatomical landmarks (see above; Table S1) were used to calculate the 2-D position of the heart as well as the position of the left and right OCs with respect to the X-Y coordinates of the heart and eyes (Figure S1D).

The trajectories of four anatomical markers (head, heart, left and right OC) were further analyzed in MATLAB to provide relevant kinematic variables (curvature of head trajectories; acceleration magnitudes of heart, eyes and OCs) that represent the animals' motion trajectory and swimming performance. A non-uniform circular mobile point kinematic model was used to describe the curved trajectories of the landmarks (Figure S1D). In this model, the trajectory of a moving point was decomposed into series of local circular trajectories (Figure S1E), defined by a particular center and radius calculated for each video frame. This kinematic model allowed distinguishing forward, lateral, centripetal and angular components of the acceleration profile for both OCs during off-center head movements produced by undulatory tail-based swimming.

High-speed video recordings and analysis of eye movements during episodes of free swimming

Sequences of individual images were analyzed offline using a custom MATLAB script. Tracking of the eyes and calculation of head-in-space and eye-in-space angular positions were performed using a semi-automatic frame-by-frame analysis as described previously [42]. Briefly, a region of interest (ROI) was drawn around each eye and processed using binary thresholding. This made the eyeball and lens to appear as two distinct black/white morphological structures. The position of each eye in space was computed as the orientation of the major axis of an ellipse, which approximates the outline of the eye [42]. The position of the head-in-space was obtained from the angle of the inter-ocular connection line between the two eyes. These values served to estimate the efficiency of compensatory eye movements during concurrent swimming-related head movements. Accordingly, the magnitude of the eye motion with respect to the head motion was determined as the ratio between the eye-in-space angle and the head-in-space angle.

Statistics

Free swimming kinematic values generated in CSV files obtained from MATLAB were analyzed using OriginPro 8 (OriginLab Corporation, USA). Data are presented as mean ± standard error of the mean (SEM) unless stated otherwise. For whisker boxplots shown in Figure 1G and Figures 2H and 2I, black circles represent 1% and 99%, respectively; black bowls represent the mean, error bars are ± SEM. Non-parametric unpaired Mann-Whitney *U*-test was used to determine significant differences between mean values (detailed statistical descriptions are provided in the respective result section and corresponding figure legends). Non-parametric Kolmogorov-Smirnov test was used to determine significant differences between data distribution (detailed statistical descriptions are provided in the respective result section and corresponding figure legends). Statistical tests were performed with Prism 7.0 (GraphPad). Eye/head motion phase relationships were calculated with Oriana 4.02 (Kovach computing services, UK).

DATA AND CODE AVAILABILITY

The accession number for the original videos and datasheets and experimental software generated through this study have been deposited to Mendeley dataset CURRENT-BIOLOGY-D-19-01330 (https://doi.org/10.17632/gn6pnsnkvm.1)